PHILOSOPHICAL TRANSACTIONS OF THE ROYAL SOCIETY B

Phil. Trans. R. Soc. B (2011) **366**, 1530–1539
doi:10.1098/rstb.2010.0345

Research

Fibre operating lengths of human lower limb muscles during walking

Edith M. Arnold[1] **and Scott L. Delp**[1,2,*]

[1]*Department of Mechanical Engineering and* [2]*Department of Bioengineering, Stanford University, Stanford, CA 94305, USA*

Muscles actuate movement by generating forces. The forces generated by muscles are highly dependent on their fibre lengths, yet it is difficult to measure the lengths over which muscle fibres operate during movement. We combined experimental measurements of joint angles and muscle activation patterns during walking with a musculoskeletal model that captures the relationships between muscle fibre lengths, joint angles and muscle activations for muscles of the lower limb. We used this musculoskeletal model to produce a simulation of muscle–tendon dynamics during walking and calculated fibre operating lengths (i.e. the length of muscle fibres relative to their optimal fibre length) for 17 lower limb muscles. Our results indicate that when musculotendon compliance is low, the muscle fibre operating length is determined predominantly by the joint angles and muscle moment arms. If musculotendon compliance is high, muscle fibre operating length is more dependent on activation level and force–length–velocity effects. We found that muscles operate on multiple limbs of the force–length curve (i.e. ascending, plateau and descending limbs) during the gait cycle, but are active within a smaller portion of their total operating range.

Keywords: muscle architecture; fibre length; simulation; musculoskeletal model; gait

1. INTRODUCTION

The force–length relationship of muscle is one of the most important and long-standing tenets of neuromuscular physiology. The force–length behaviour of muscle fibres was described in 1966 based on measurements of maximal isometric force generated by the semitendinosus in the frog [1]. These experiments revealed that when fibres are shorter than optimal length, the force a muscle generates when maximally activated increases with fibre length (the ascending limb of the force–length curve). Beyond the optimal length, the maximal active force a muscle generates decreases with fibre length (the descending limb of the force–length curve), and the muscle generates passive force [2]. Near optimal fibre length, the muscle generates relatively consistent force when maximally activated (the plateau of the force–length curve). Thus, the length of muscle fibres profoundly affects the muscle's force-generating capacity.

Muscle force is also affected by muscle fibre velocity. When fibres shorten during activation (concentric), force generation decreases with increasing shortening velocity [3]. When fibres lengthen during activation (eccentric), force generation increases with lengthening velocity. This increase in force is most pronounced at low lengthening velocities; at high lengthening velocity, the increase in lengthening velocity has less effect on force production [4]. Muscle force also depends on the level of activation, history-dependent effects, fatigue and other factors [5,6].

To understand muscle function during gait in terms of the force–length and force–velocity properties, it is necessary to characterize the lengths of muscle fibres relative to their optimal length. However, it is difficult to measure the operating length of muscle fibres (i.e. the lengths of muscle fibres relative to optimal fibre length) during gait. Direct determination of fibre operating length requires measurement of sarcomere length. Sarcomere length can be measured by laser diffraction [7], which has been used to study operating lengths of muscles in the upper extremity [8]. However, this laser diffraction requires surgery to visualize the muscle fibres and sarcomeres. Microendoscopy is less invasive than laser diffraction and enables direct measurement of sarcomere lengths [9], but this technique has not yet been adapted for use during human locomotion. As a result, there are no direct measurements of human sarcomere and fibre operating lengths during human locomotion.

Several studies have estimated the sarcomere or fibre operating lengths of lower limb muscles during motion. Cutts [10] estimated sarcomere lengths for the semimembranosus, semitendinosus, biceps femoris long head (BFLH), rectus femoris, vastus lateralis and vastus medialis at an anatomical position and used these values with cine film of two subjects walking to estimate sarcomere length at five points during the gait cycle [11]. This approach provided valuable insights but did not include the effects of muscle–tendon dynamics

* Author for correspondence (delp@stanford.edu).

One contribution of 15 to a Theme Issue 'Integration of muscle function for producing and controlling movement'.

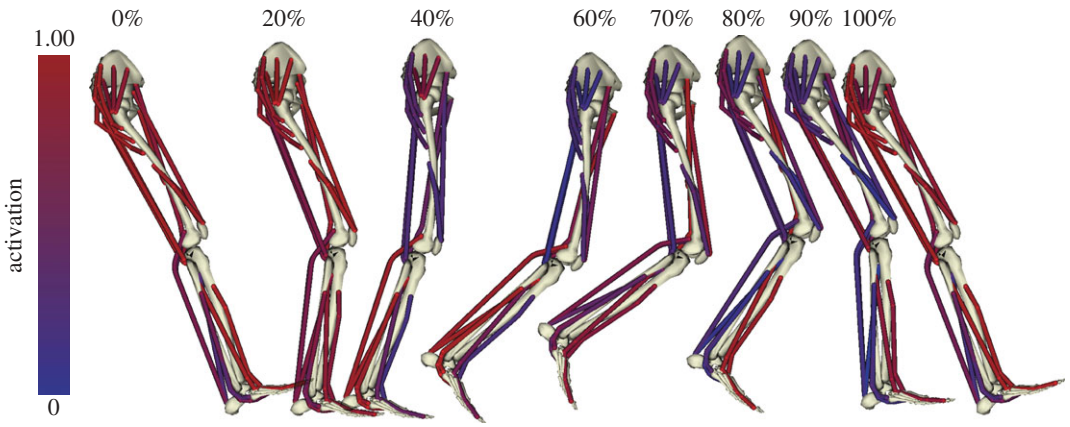

Figure 1. Three-dimensional musculoskeletal model of the lower limb during one gait cycle. Bony geometry includes the phalanges, metatarsals, calcaneus, talus, fibula, tibia, patella, femur and pelvis. Joint angles and angular velocities were calculated for 10 gait cycles and then averaged over a common basis of 0–100% to produce one characteristic gait cycle beginning and ending at heel strike. Muscle-tendon actuators representing lower limb muscles were constrained to origin and insertion points and wrapping surfaces. Typical muscle activation patterns for walking were prescribed for each muscle on a 0.00 to 1.00 scale, representing 0 to 100% activation.

(e.g. force–velocity effects and musculotendon compliance). Other studies have estimated fibre or fascicle lengths over a range of motion for a single joint [12–18] or during a movement [19] using imaging technology or mathematical modelling. Fukunaga *et al.* [19], for example, used ultrasound measurements to examine muscle fascicle lengths and tendon lengths of medial gastrocnemius. They found that muscle fascicles experienced less change in length than the muscle–tendon complex because the tendon took up some of the length change. This occurs because the long, compliant tendon of the medial gastrocnemius stretches when the muscle is activated and muscle force is developed. The effect of tendon stretch on muscle fascicle length is greatest in muscles with high musculotendon compliance (i.e. large ratio of tendon slack length to optimal muscle fibre length [5,20]). It is important to note that without measurements of sarcomere length, previous studies of lower limb muscles could only roughly approximate fibre operating lengths [21].

Two recent advances enable more accurate estimation of muscle fibre operating lengths in human lower limb muscles during locomotion over earlier methods. First, Ward *et al.* [22] reported measurements of muscle architecture of lower limb muscles. These measurements include fibre and sarcomere length at known joint angles. Second, Arnold *et al.* [23] developed a computer model of the lower extremity musculoskeletal system based on the architectural measurements of Ward *et al.* [22]. This model characterizes the muscle–tendon paths and force-generating properties for lower limb muscles and allows detailed examination of muscle fibre and tendon dynamics for 28 muscles that are based on the data of Ward *et al.* [22].

The goal of this study was to calculate the fibre operating lengths of human lower limb muscles during walking. We used a computer simulation of muscle–tendon dynamics to address three questions. First, what are the effects of musculotendon compliance and muscle activation on fibre operating lengths? Second, on which limbs of the force–length curve (ascending limb, descending limb and plateau) do lower limb muscles operate when they are most active during the gait cycle? Third, when they are active, which exhibit eccentric, concentric or isometric behaviour during walking?

2. METHODS

We used a computer model of the musculoskeletal system that represents the geometry of the bones, the kinematics of joints, and the lines of action and force-generating properties of lower limb muscles (figure 1). Given patterns of muscle activations and joint angles, the musculoskeletal model calculates the muscle–tendon lengths, muscle forces, tendon strains and muscle fibre lengths in a dynamic simulation. We used experimentally measured muscle activations and joint angles to estimate muscle fibre operating lengths during walking, and evaluated how variations in muscle activations and musculotendon compliance affect muscle fibre operating lengths. An overview of the musculoskeletal model and methods to compute muscle fibre lengths is provided below.

(a) *Musculoskeletal model*

The model included the geometry of the bones of the lower limb and pelvis, created by digitizing the bones of a male subject [20,24]. The bone dimensions represented a 170 cm tall male [25]. The model also included representations of the ankle, knee and hip joints that defined motions between the bones. The ankle was a revolute joint between the tibia and talus defined by 1 degree of freedom (dorsiflexion/plantarflexion) [26]. The knee had a single degree of freedom (flexion/extension) and used the equations reported by Walker *et al.* [27] and Delp [28] to define the translations and rotations between the femur, tibia and patella as functions of knee flexion angle. The hip was a ball and socket joint with 3 degrees of freedom (flexion/extension, adduction/abduction, and internal/external rotation). Thus, each leg in the model had 5 degrees of freedom.

The model included 35 muscles of the lower limb. Line segments approximated the muscle–tendon path

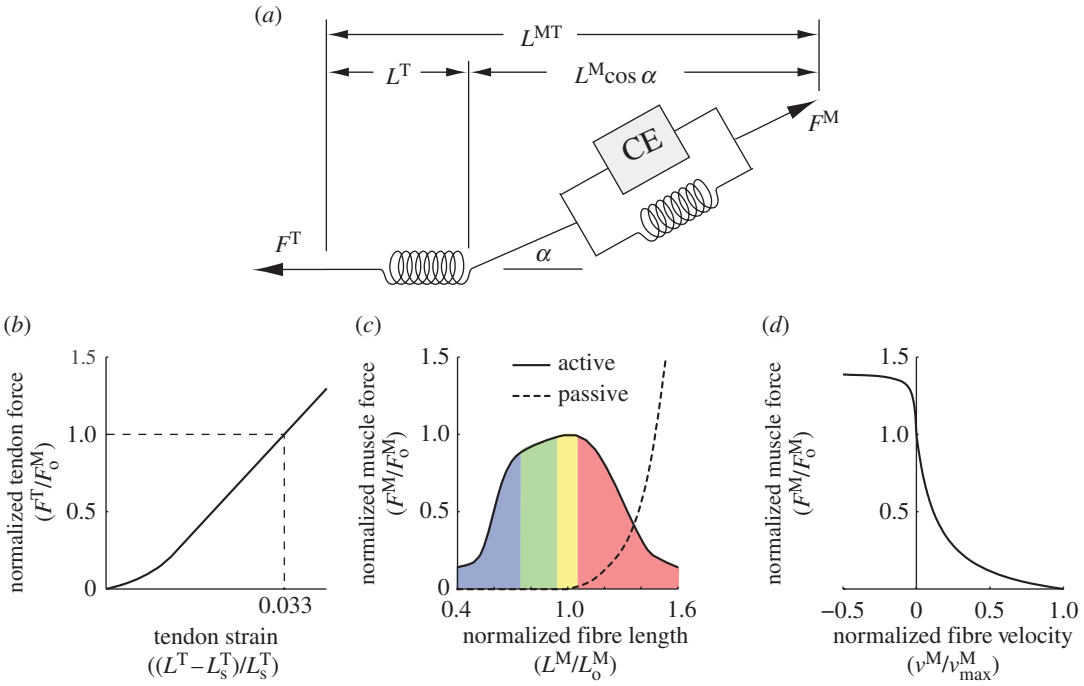

Figure 2. Lumped parameter model of muscle used to simulate tendon and muscle dynamics [5]. (*a*) The muscle–tendon length (L^{MT}) derived from the muscle–tendon geometry was used to compute muscle fibre length (L^{M}), fibre shortening velocity (v^{M}), tendon length (L^{T}), pennation angle (α), muscle force (F^{M}) and tendon force (F^{T}). Muscle was represented as a passive elastic element in parallel with an active contractile element (CE). Tendon was represented as a nonlinear elastic element. (*b*) Tendon force–strain relationship assumed that the strain in tendon ($(L^{T}-L^{T}_{s})/L^{T}_{s}$) was 0.033 when the muscle generated maximum isometric force (F^{M}_{o}). (*c*) Normalized active and passive force–length curves were scaled by maximum isometric force (F^{M}_{o}) and optimal fibre length (L^{M}_{o}) derived from experimental measurements for each muscle. The regions of the active force–length curve were described as the steep ascending limb (blue), shallow ascending limb (green), plateau (yellow) and descending limb (red). (*d*) The force–velocity curve included concentric ($v^{M} > 0$) and eccentric ($v^{M} < 0$) regions and was scaled by maximum isometric force and v^{M}_{max} of $10 \cdot L^{M}_{o}\,s^{-1}$.

from the origin to insertion. In the case of muscles with broad attachments (e.g. gluteus medius), multiple muscle paths were used, resulting in 44 muscle–tendon compartments. Muscle–tendon paths that wrapped over bones, deeper muscles or retinacula included these anatomical constraints [23]. The model of musculoskeletal geometry enables calculations of muscle–tendon lengths (i.e. origin to insertion path length) and moment arm of each muscle–tendon complex. To compute muscle fibre length, we used a model of muscle–tendon contraction dynamics [29].

We used a lumped parameter model to characterize muscle–tendon contraction dynamics [5] (figure 2*a*). This model included four parameters (optimal fibre length, maximum isometric force, pennation angle and tendon slack length) that scale generic properties of muscle and tendon to represent the architecture of each muscle–tendon unit. The model of tendon represents the nonlinear elastic properties of tendon. The tendon force–strain relationship (figure 2*b*) was scaled to represent a specific muscle–tendon complex by tendon slack length (L^{T}_{s}) and peak muscle force (F^{M}_{o}). Tendon strain was assumed to be 0.033 when muscle generated its peak isometric force [5]. The model of muscle included the active and passive force–length relationships (figure 2*c*), which were scaled by each muscle's optimal fibre length (L^{M}_{o}) and peak isometric force (F^{M}_{o}) [5]. The force–velocity relationship (figure 2*d*) was also included: the maximum shortening velocity of each muscle was assumed to be 10 optimal fibre lengths per second (i.e. $v^{M}_{max} = 10 \cdot L^{M}_{o}\ s^{-1}$) [5].

The parameters used to scale properties of each muscle–tendon unit included in this study were derived from measurements of muscle architecture in 21 cadavers reported by Ward *et al.* [22]. The cadavers from which muscle architecture parameters were measured had an average height of 168.4 ± 9.3 cm and mass of 82.7 ± 15.2 kg. Optimal fibre lengths and pennation angles were taken directly from Ward *et al.* [22]. Maximum isometric forces were calculated from the measured physiological cross-sectional area as described by Arnold *et al.* [23]. As Ward and co-workers measured fibre lengths and sarcomere lengths at a known body position, we set the tendon slack length of each muscle–tendon complex such that the fibre length and sarcomere length of each muscle in the model was the same as the experimental measurements when the model was in the equivalent configuration.

The accuracy of the musculoskeletal model was verified by comparing the moment arms of muscles to those measured in cadaver subjects [30–32] and maximum moments generated by each muscle group to moments generated by an earlier model [20] and reported in experimental data [33–39], as described by Arnold *et al.* [23].

(b) *Computation of fibre lengths during walking*

We produced a simulation of muscle–tendon dynamics during walking to estimate muscle fibre operating lengths. The simulation prescribed experimental joint angles measured from a subject walking on a treadmill. The subject was a healthy male (height 1.83 m, mass 65.9 kg) who walked continuously at a self-selected speed of 1.36 m s^{-1}. The positions of 41 markers [40] were measured using a six-camera motion capture system (Motion Analysis Corporation, Santa Rosa, CA, USA). The ground reaction forces were measured using a force-plate-instrumented treadmill (Bertec Corporation, Columbus, OH, USA).

We scaled the model to the anthropometry of the subject based on marker locations. Optimal fibre length and tendon slack length were scaled with muscle–tendon length so that they maintained the same ratio (i.e. $L_o^M : L_s^T$ was maintained). Virtual markers were placed on the model to match the locations of the experimental markers and an inverse kinematics algorithm was used to determine the joint angles of the model over 10 complete gait cycles [41,42]. Ten right-side gait cycles were segmented using the measured ground reaction force to identify heel strike. The gait cycles were normalized over a 0–100% scale and averaged to obtain a characteristic gait cycle for the subject.

The characteristic gait cycle was compared with an experimental study of multiple subjects [40] to confirm that the kinematics were typical. The time period of the characteristic gait cycle was 1.1 s and toe-off occurred at 66 per cent, which is slightly later than the reference study [40]. To account for this difference, the stance and swing phases of the reference study were renormalized so that the stance and swing percentages matched our characteristic gait cycle. The joint angles of interest in this study—hip flexion, hip adduction, knee flexion and ankle plantarflexion—were comparable with the joint angles reported by Kadaba *et al.* (figure 3) with some differences owing to discrepancies in the definitions of joint angles and coordinate systems.

We produced a dynamic simulation of muscle–tendon dynamics during walking using the biomechanics software, OpenSim v. 2.0.2 [42]. We prescribed muscle-activation patterns and joint kinematics, and calculated the muscle forces and fibre lengths that satisfied these constraints. To study the effects of muscle activation and musculotendon compliance on fibre operating lengths, we produced simulations with three different activation cases: maximum activation, minimum activation and typical activation during gait [43]. In our muscle model, activation was a value between 0.00 and 1.00 (i.e. 0–100% of maximum). In the maximum activation case, activation was 1.00 in all muscles. For the minimum activation case, it was not possible to prescribe 0.00 activation for the simulation of walking because the fibres must maintain tension while the muscle–tendon complex is shortening. Thus, activation was the smallest value that maintained tension in the muscle fibres over the entire gait cycle. Minimum activation was typically 0.05, however muscles that reached very high shortening velocities—soleus, the gastrocnemeii, semimembranosus and rectus femoris—demanded higher values (0.10 or 0.15). In the typical activation case, we prescribed activations of muscles based on electromyography (EMG) data reported by Winter [43]. We normalized the EMG data so that the mean peak average was equal to 1.00 [44].

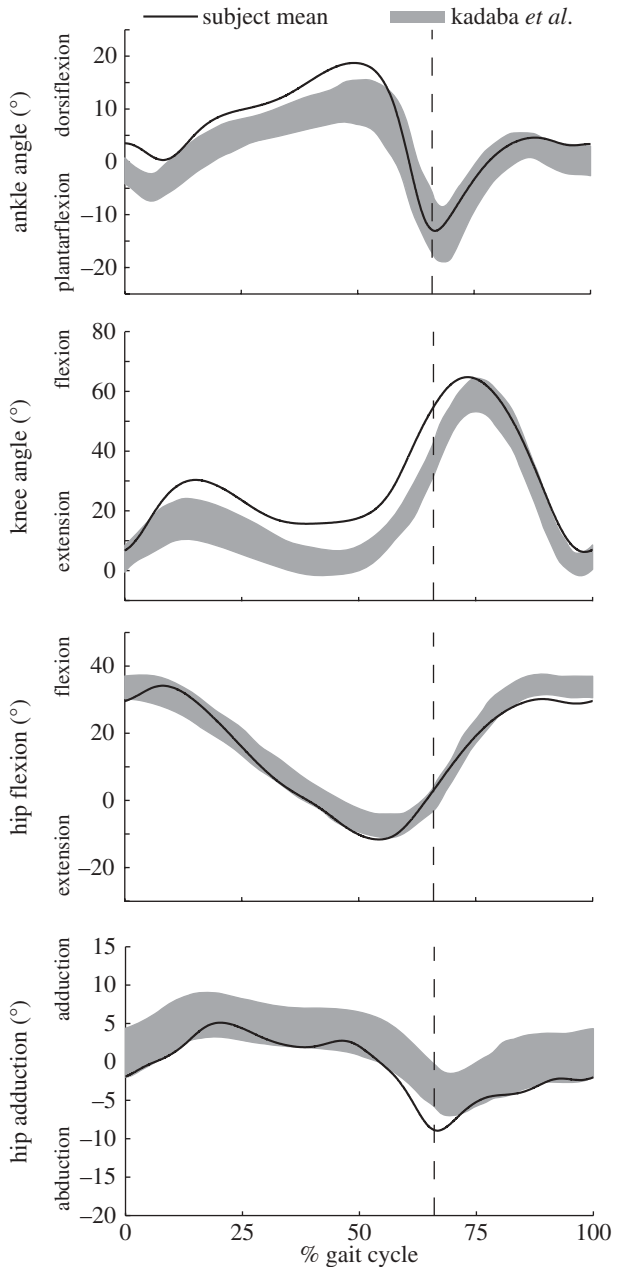

Figure 3. Joint angles prescribed for the simulation. The kinematics of the subject's characteristic gait cycle (solid lines) were calculated as the average of 10 consecutive gait cycles. These joint angles were compared with those reported by Kadaba *et al.* [40], ±1 s.d., which were adjusted so that the timing of toe-off (dashed line) aligned with our subject (shaded region). Joint angles were comparable with some discrepancies owing to variation in the definitions of joint angles and coordinate frames.

We included 17 important lower limb muscles in our simulation and calculated normalized fibre length during gait with minimum and maximum activation to determine the feasible operating region. We calculated the trajectory of normalized fibre length during gait for each muscle using the typical activation pattern [43] and compared it with the force–length curve. Over the gait cycle, the trajectory of normalized fibre

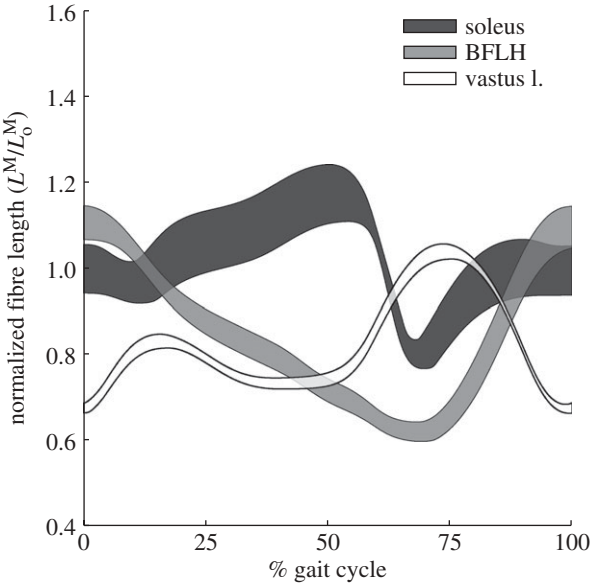

Figure 4. Feasible operating region of normalized fibre length for soleus, BFLH and vastus lateralis during one gait cycle. For the prescribed joint angles, any activation pattern will produce a trajectory of normalized fibre length in this range. The feasible operating region for each muscle is the difference between fibre length trajectories during gait for minimum and maximum activation. Muscles with long tendons relative to their optimal fibre length (i.e. large values of $L_s^T : L_o^M$) have wider feasible operating ranges than muscles with relatively short tendons.

length was described in terms of four limbs of the force–length curve [45] bounded by values of normalized length that corresponded to meaningful changes in slope for the sarcomere force–length curve [46] and the model force–length curve [23,42]: the steep ascending limb ($L^M/L_o^M < 0.75$), the shallow ascending limb ($0.75 \leq L^M/L_o^M < 0.95$), the plateau ($0.95 \leq L^M/L_o^M \leq 1.05$) and the descending limb ($1.05 < L^M/L_o^M$), as illustrated in figure 2*d*.

3. RESULTS

(a) *Effects of musculotendon compliance and activation on fibre operating lengths*

Musculotendon compliance increased the difference between the normalized fibre length trajectories for the minimum and maximum activation cases (figure 4). High musculotendon compliance (i.e. high $L_s^T : L_o^M$ ratio) produced a wide operating region (i.e. the region bound by the minimum and maximum activation cases) across the gait cycle. A wider operating region indicated that activation pattern could have a strong effect on the trajectory of fibre operating length. Low musculotendon compliance produced a narrow operating region; in these cases, the operating length was less sensitive to the level of muscle activation and force. Figure 4 shows these regions for a selection of muscles with different $L_s^T : L_o^M$ ratios. Soleus, which has a relatively long, compliant tendon (table 1), had a wide operating region. BFLH and vastus lateralis had moderate and low musculotendon compliance, and their operating regions were correspondingly narrower.

Musculotendon compliance also affected fibre length by interacting with the force–velocity property of muscle. For example, during mid-stance, the fibres of the medial gastrocnemius underwent an eccentric contraction. High fibre force increased tendon strain and the fibres were correspondingly shorter than they would have been with the same activation and joint configuration in static equilibrium (figure 5). During terminal stance, the fibres of medial gastrocnemius shortened rapidly, producing less than isometric force. Thus, tendon strain was reduced and the fibres were longer than they would have been in static equilibrium.

Table 1. Muscle fibre and tendon length modelling parameters scaled to subject geometry.

	compliance ratio $L_s^T : L_o^M$	tendon slack length L_s^T (cm)	optimal fibre length L_o^M (cm)
medial gastrocnemius	7.8	44.7	5.7
peroneus longus	6.6	36.1	5.5
lateral gastrocnemius	6.5	42.6	6.6
soleus	6.4	31.6	4.9
extensor digitorum longus	5.3	39.6	7.5
semimembranosus	5.1	36.5[a]	7.2
rectus femoris	4.6	37.1	8.1
tibialis anterior	3.5	26.5	7.5
biceps femoris long head	3.3	33.8	10.2
peroneus brevis	3.2	16.2	5.0
vastus lateralis	1.3	14.5	11.1
semitendinosus	1.3	25.9	20.4
adductor longus	1.2	13.4	11.2
vastus medialis	1.2	12.6	10.9
gluteus medius	0.9	6.6	7.3
gluteus maximus	0.5	7.4	15.9
sartorius	0.3	11.5	42.1

[a] L_s^T for semimembranosus is based on an unscaled value of 34.8 cm, consistent with the value predicted by the architecture data from Ward *et al.* [22]. This differs from the value listed in Arnold *et al.* [23], which was adjusted for high hip-flexion postures.

(b) *Fibres operate on multiple limbs of force–length curve*

All but one of the muscles analysed operated on multiple limbs of the force–length curve during the gait cycle (figure 6). Medial gastrocnemius, lateral gastrocnemius, semimembranosus, rectus femoris and BFLH operated on the ascending limbs, plateau and descending limb. Biarticular muscles with short fibres and large moment arms had the largest range of normalized fibre lengths over the gait cycle. For example, soleus and medial gastrocnemius are plantarflexors with similar fibre lengths and moment arms. Their operating length trajectories were similar, but soleus stopped shortening on the shallow region of the ascending limb, whereas medial gastrocnemius shortened onto the steep ascending limb when the knee flexed and ankle plantarflexed in terminal stance. Semimembranosus operated over a large range of length. By contrast, semitendinosus, which has a similar moment arm but longer fibres, covered a much smaller range of length.

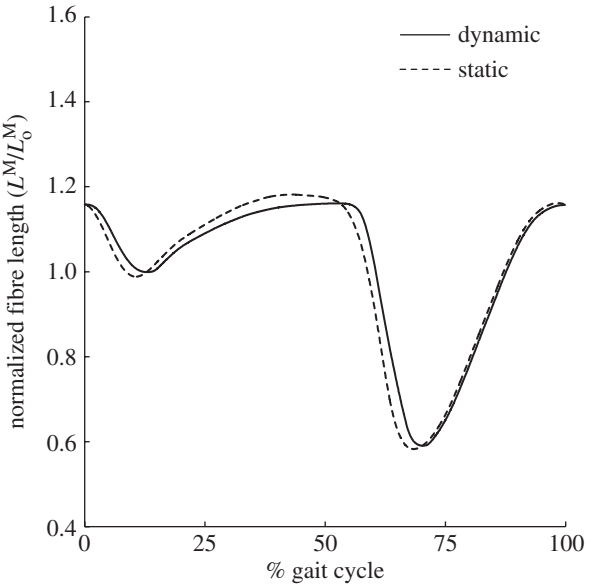

Figure 5. Effect of force–velocity property on trajectory of normalized fibre length in medial gastrocnemius. Increased force in eccentric contraction and decreased force in concentric contraction, compared with isometric contraction, alter tendon strain. As a result, normalized fibre length calculated with a dynamic simulation (solid line) was shorter in eccentric contraction and longer in concentric contraction than would be determined from a static calculation (dashed line).

Only one muscle, sartorius, was confined to a single limb of the force–length curve. Sartorius has long fibres and is the only biarticular muscle that flexes the hip and the knee. While the combination of hip and knee angles during walking stretched and shortened muscles that extend the knee and flex the hip to their extremes, sartorius experienced relatively little change in muscle–tendon length during the gait cycle.

(c) *Fibres are active on a subsection of their operating range*

Muscles whose range of normalized fibre length over the gait cycle reached multiple limbs of the force–length curve were typically confined to a smaller range of lengths when they were active. For example, BFLH reached all four limbs of the force–length curve but normalized fibre length when the muscle was active (during early stance and late swing) fell on the descending limb and plateau. Of the eight muscles that operated on the steep ascending limb, only three were active in that region: rectus femoris, vastus lateralis and vastus medialis. The plateau and descending limb were the sites of the most activity.

(d) *Active fibres show eccentric, isometric and concentric behaviour*

We observed all three types of contraction—eccentric, isometric and concentric—in the operating length trajectories. Ten muscles exhibited stretch-shortening behaviour, beginning their period of activation eccentrically, reaching a maximum length and continuing concentrically. BFLH, semitendinosus and semimembranosus behaved this way on the plateau and descending limbs in the swing-to-stance transition. Vastus medialis and lateralis did so on the steep and shallow ascending limbs. Sartorius was the only muscle to show shortening-stretch behaviour. Few muscles shortened rapidly during activation, and those that did (e.g. soleus and the gastrocnemeii) were near optimal length during this time. The highest speed eccentric contractions occurred in the muscles that were active on the steep ascending limb (rectus femoris, vastus lateralis and vastus medialis). Musculotendon compliance caused fibre velocity to stay closer to zero than the muscle–tendon complex as a whole in several cases. This is observable in figure 6 as the trajectory of normalized fibre length diverging from the upper boundary of the feasible operating region (e.g. soleus and extensor digitorum longus in stance; semimembranosus and biceps femoris longus in swing).

4. DISCUSSION

Comparing the feasible operating region and the trajectory of normalized fibre lengths during gait of 17 lower limb muscles revealed three aspects of their fibre dynamics. First, high musculotendon compliance resulted in increased sensitivity of the trajectory of normalized fibre length during gait to muscle activation pattern and the force–velocity property. Second, muscles operate on multiple limbs of the force–length curve during the gait cycle, yet are typically active on a smaller subsection of this range. Third, eccentric, concentric and isometric behaviours were observed during active periods.

Muscles with higher musculotendon compliance showed a larger difference between minimum and maximum activation cases. Thus, in muscles with a wide feasible operating region, the particular activation pattern can have a larger effect than in those with a narrow range. Additionally, musculotendon compliance is linked to the influence of the force–velocity relationship when muscles are active. In eccentric activation, the higher force generation increases tendon strain and fibres are correspondingly shorter than they would be in a static posture with the same activation. The opposite occurs during concentric activation. In the plantarflexors, these properties have the effect of slowing fibre-lengthening velocity when the muscle–tendon complex is lengthening and so normalized fibre length does not travel very far down the descending limb. This finding illustrates the importance of including the force–velocity property in the muscle model and creating a dynamic simulation, as we have done here.

Though many muscles reached multiple regions of the force–length curve during the gait cycle, they were active over a much smaller range of lengths. Most muscles acted on the plateau or descending limb. The notable exceptions are the vasti and rectus femoris in early stance. A common thread for these muscles at these times is that they act in a braking capacity. The vasti and rectus femoris prevent the knee from buckling [47] and brake the mass centre [48]. It has been proposed that the ascending limb of the force–length curve is inherently mechanically stable [45,46], a property that would be beneficial for braking.

In biarticular muscles, the range of normalized fibre lengths over the gait cycle tends to be larger than similarly

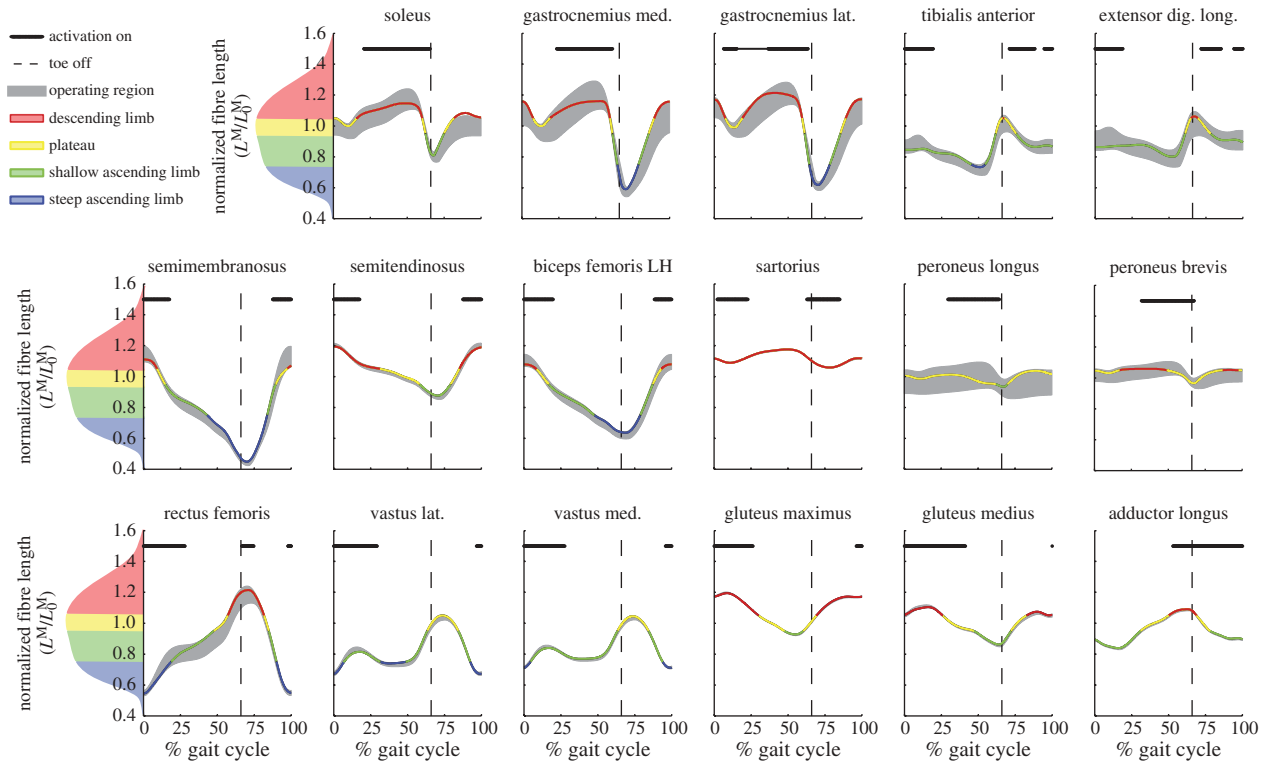

Figure 6. Trajectory of normalized fibre length, feasible operating region and the period of activation during gait for 17 lower limb muscles. The feasible operating regions (grey) were calculated for minimum to maximum activation. Trajectories of normalized fibre length were calculated for the activation pattern reported by Winter [43] (solid, multi-coloured line). The colours of the curve correspond to the limbs of the force–length curve shown on the far left of each row. Portions of the gait cycle when a muscle's activation exceeded its mean value for the gait cycle are indicated at the top of each plot (thick black line). Toe-off is indicated at 66% (dashed line).

located uniarticular muscles (e.g. gastrocnemius compared to soleus). Consequently, these biarticular muscles experience very high shortening velocities. The notable exception to this biarticular trend was sartorius. As it is a hip flexor and knee flexor, the effect of biarticular motion is to reduce the total operating range.

There are few reports of human sarcomere or fibre operating ranges with which to compare our results. Calculation of force–length relationships of rectus femoris [49], soleus and tibialis anterior [14] based on measurements of maximum voluntary joint moments indicate that over a range of joint angles these muscles operate on the ascending limb and plateau of the force–length curve. Our results, however, indicate that muscles frequently operate on the descending limb and are often active at these longer lengths.

Insights into fibre and sarcomere lengths during human walking are sparse, but studies by Cutts [11] and Fukunaga *et al.* [19] provide useful comparisons. Cutts calculated sarcomere length for muscles crossing the knee at five time points during a gait cycle [11] using a method that predicted sarcomere length based on changes in muscle–tendon length and assuming a rigid tendon [10]. The shapes of the curve formed by these points agree with our results and the regions on which semimembranosus and rectus femoris operate are similar. However, our results for semitendinosus and the vasti indicate longer and shorter operating lengths, respectively, than predicted by Cutts [11].

Fukunaga *et al.* [19] used ultrasonography to determine the relative change in length of the muscle fascicles, tendon and muscle–tendon complex of gastrocnemius medialis. They found that fascicle length was near constant during the single-limb support phase, even as the muscle–tendon complex was lengthening, a result which our study confirms. Furthermore, though their approach precluded the precise determination of normalized fibre length, they estimated that the active range of gastrocnemius medialis would correspond to sarcomere lengths of 2.75–2.92 μm. Though our results indicate somewhat longer sarcomere lengths, this supports our finding that when this muscle is active during walking, it is on the plateau and descending limb.

In this study, we combined a musculoskeletal model of the lower limb with experimental joint angles and typical activation patterns to produce a forward dynamic simulation of muscle fibre behaviour during walking. A key component of this approach is the architecture data [22] used to create the model. Without experimental data that made an explicit link between fibre length and joint angle, the model could not precisely capture the relation between fibre length and a functional motion.

This approach overcomes many of the challenges in earlier models and experimental methods, but has several limitations. We used a generic model scaled to a single subject and joint angles averaged over multiple gait cycles. Our subject had no gait pathologies but exhibited high knee flexion throughout the stance phase. Had he walked with a more extended knee the fibres of the vasti and rectus femoris would be slightly shorter and the fibres of the hamstrings and

gastrocnemeii would be slightly longer. Differences between an individual's muscle architecture and the model or subject-to-subject variation in activations or kinematics could affect the results. Operating range may also be affected by subject activity; a prior study reported variation in the force–length property of rectus femoris between cyclists, runners and non-athletes [49–51]. Future work should extend the computational methods described here to experimental data from multiple subjects walking at a variety of speeds with subject-specific EMG patterns to determine whether the results of this study are particular to this subject or represent the general paradigm for muscle function during walking.

We simplified our model by assuming that all muscles had identical material properties—tendon strain at maximum isometric muscle force was 0.033 and muscle generated passive tension when fibres exceeded optimal length [5]—even though these properties may vary among muscles [5,52]. Our results demonstrate the effects of musculotendon compliance (i.e. the ratio of tendon slack length to optimal fibre length) on fibre lengths during walking, but they do not show the effects of tendon stiffness. Tendon stiffness (K^{T}) is the product of the tendon elastic modulus (E^{T}) and cross-sectional area (A^{T}) divided by tendon slack length (L_{s}^{T}), i.e. $K^{T} = E^{T}A^{T}/L_{s}^{T}$. The tendons of the plantarflexors may be less stiff than other muscles [53]. To examine how this lower tendon stiffness affects the fibre trajectory of the soleus, we increased the tendon strain at maximum isometric muscle force to 0.066 (halving the stiffness). This decreased tendon stiffness produced a wider operating region and a normalized fibre length trajectory that was more isometric and closer to the plateau of the force–length curve than was observed for the default tendon stiffness (figure 7). Future work will examine the effect of tendon material properties on the normalized fibre length trajectories and operating regions for other muscles.

There are also limitations inherent in the muscle model used. In the application of experimental architecture data [22] to the model [23], we assumed that optimal sarcomere length for all muscles is 2.7 μm. There is evidence that optimal sarcomere length may vary between muscles [54], but without knowledge of each muscle's optimal length, a single length of 2.7 μm is a reasonable assumption. Additionally, the lumped parameter muscle model assumes that all fibres within a muscle operate at the same length. The fibres of these muscles may be distributed over a range of lengths [15,55–57]. In this case, the fibres within a muscle may occupy different regions of the force–length curve or operate at varying velocities. Additionally, the computational implementation of the model [29] had numerical limitations when fibre-shortening velocity was high and activation was low.

Despite these limitations, this study sheds new light on the structure–function relationships of lower limb muscles during walking. Future investigation is important from both scientific and clinical perspectives. Identifying normal structure–function relationships may aid with surgical planning for gait pathologies such as crouch gait, where treatments such as tendon transfer or lengthening may have a profound effect on musculoskeletal structure [58].

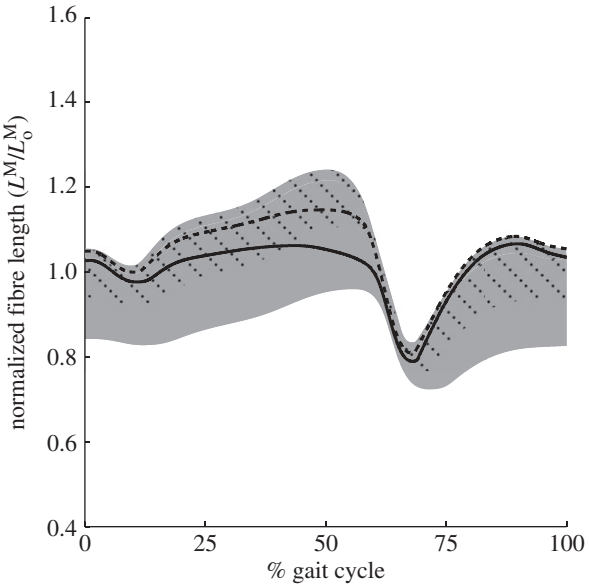

Figure 7. Effect of tendon stiffness on trajectory of normalized fibre length and feasible operating region. The default tendon force–strain relationship was altered in soleus so that the tendon was half as stiff (i.e., tendon strain was 0.066 at peak isometric muscle force). Compared to the default operating region (dotted area) and trajectory of normalized fibre length (dashed line) modelling soleus with half the tendon stiffness reduces the lower limit of the operating region (grey area) and produces shorter, more isometric fibre length (solid line) when the muscle is active.

The authors thank Sam Ward for assistance in integrating his data for muscle architecture into the lower limb model; Chand John and Jill Higginson for data collection; Ayman Habib, Ajay Seth, Pete Loan and Samuel Hamner for their assistance in developing this simulation; and Melinda Cromie, James Dunne, Melanie Fox, Kathryn Keenan and Gabriel Sanchez for their valuable feedback. This work is supported by a Stanford Bio-X Graduate Student Fellowship and the National Institutes of Health NIH Grants U54 GM072970 and R01 HD033929.

REFERENCES

1 Gordon, A. M., Huxley, A. F. & Julian, F. J. 1966 The variation in isometric tension with sarcomere length in vertebrate muscle fibres. *J. Physiol.* **184**, 170–192.
2 Magid, A. & Law, D. J. 1985 Myofibrils bear most of the resting tension in frog skeletal muscle. *Science* **230**, 1280–1282. (doi:10.1126/science.4071053)
3 Bahler, A. S., Fales, J. T. & Zierler, K. L. 1968 The dynamic properties of mammalian skeletal muscle. *J. Gen. Physiol.* **51**, 369–384. (doi:10.1085/jgp.51.3.369)
4 Joyce, G. C. & Rack, P. M. 1969 Isotonic lengthening and shortening movements of cat soleus muscle. *J. Physiol.* **204**, 475–491.
5 Zajac, F. E. 1989 Muscle and tendon: properties, models, scaling, and application to biomechanics and motor control. *Crit. Rev. Biomed. Eng.* **17**, 359–411.
6 Herzog, W., Lee, E. J. & Rassier, D. E. 2006 Residual force enhancement in skeletal muscle. *J. Physiol.* **574**, 635–642. (doi:10.1113/jphysiol.2006.107748)
7 Fleeter, T. B., Adams, J. P., Brenner, B. & Podolsky, R. J. 1985 A laser diffraction method for measuring muscle

sarcomere length *in vivo* for application to tendon transfers. *J. Hand Surg. Am.* **10**, 542–546.
8 Lieber, R. L. & Friden, J. 1998 Musculoskeletal balance of the human wrist elucidated using intraoperative laser diffraction. *J. Electromyogr. Kinesiol.* **8**, 93–100. (doi:10.1016/S1050-6411(97)00025-4)
9 Llewellyn, M. E., Barretto, R. P., Delp, S. L. & Schnitzer, M. J. 2008 Minimally invasive high-speed imaging of sarcomere contractile dynamics in mice and humans. *Nature* **454**, 784–788.
10 Cutts, A. 1988 The range of sarcomere lengths in the muscles of the human lower limb. *J. Anat.* **160**, 79–88.
11 Cutts, A. 1989 Sarcomere length changes in muscles of the human thigh during walking. *J. Anat.* **166**, 77–84.
12 Fukunaga, T., Ichinose, Y., Ito, M., Kawakami, Y. & Fukashiro, S. 1997 Determination of fascicle length and pennation in a contracting human muscle *in vivo*. *J. Appl. Physiol.* **82**, 354–358.
13 Chleboun, G. S., France, A. R., Crill, M. T., Braddock, H. K. & Howell, J. N. 2001 *In vivo* measurement of fascicle length and pennation angle of the human biceps femoris muscle. *Cells Tissues Organs* **169**, 401–409. (doi:10.1159/000047908)
14 Maganaris, C. N. 2001 Force–length characteristics of *in vivo* human skeletal muscle. *Acta Physiol. Scand.* **172**, 279–285. (doi:10.1046/j.1365-201x.2001.00799.x)
15 Herzog, W., Hasler, E. & Abrahamse, S. K. 1991 A comparison of knee extensor strength curves obtained theoretically and experimentally. *Med. Sci. Sports Exerc.* **23**, 108–114.
16 Winter, S. L. & Challis, J. H. The force–length curves of the human rectus femoris and gastrocnemius muscles *in vivo*. *J. Appl. Biomech.* **26**, 45–51.
17 Winter, S. L. & Challis, J. H. The expression of the skeletal muscle force–length relationship *in vivo*: a simulation study. *J. Theor. Biol.* **262**, 634–643. (doi:10.1016/j.jtbi.2009.10.028)
18 Griffiths, R. I. 1991 Shortening of muscle fibres during stretch of the active cat medial gastrocnemius muscle: the role of tendon compliance. *J. Physiol.* **436**, 219–236.
19 Fukunaga, T., Kubo, K., Kawakami, Y., Fukashiro, S., Kanehisa, H. & Maganaris, C. N. 2001 *In vivo* behaviour of human muscle tendon during walking. *Proc. R. Soc. Lond. B* **268**, 229–233. (doi:10.1098/rspb.2000.1361)
20 Delp, S. L., Loan, J. P., Hoy, M. G., Zajac, F. E., Topp, E. L. & Rosen, J. M. 1990 An interactive graphics-based model of the lower extremity to study orthopaedic surgical procedures. *IEEE Trans. Biomed. Eng.* **37**, 757–767. (doi:10.1109/10.102791)
21 Ettema, G. J. 1997 Gastrocnemius muscle length in relation to knee and ankle joint angles: verification of a geometric model and some applications. *Anat. Rec.* **247**, 1–8. (doi:10.1002/(SICI)1097-0185(199701)247:1<1::AID-AR1>3.0.CO;2-3)
22 Ward, S. R., Eng, C. M., Smallwood, L. H. & Lieber, R. L. 2009 Are current measurements of lower extremity muscle architecture accurate? *Clin. Orthop. Relat. Res.* **467**, 1074–1082. (doi:10.1007/s11999-008-0594-8)
23 Arnold, E. M., Ward, S. R., Lieber, R. L. & Delp, S. L. 2010 A model of the lower limb for analysis of human movement. *Ann. Biomed. Eng.* **38**, 269–279. (doi:10.1007/s10439-009-9852-5)
24 Arnold, A. S., Asakawa, D. J. & Delp, S. L. 2000 Do the hamstrings and adductors contribute to excessive internal rotation of the hip in persons with cerebral palsy? *Gait Posture* **11**, 181–190. (doi:10.1016/S0966-6362(00)00046-1)
25 Gordon, C. C., Churchill, T., Clauser, C. E., Bradtmiller, B., McConville, J. T., Tebbetts, I. & Walker, R. A. 1988 *Anthropometric survey of U.S. Army personnel: methods and summary statistics*. Natick, MA: United States Army Natick Research, Development, and Engineering Center.
26 Inman, V. T. 1976 *The joints of the ankle*. Baltimore, MD: Williams & Wilkins.
27 Walker, P. S., Rovick, J. S. & Robertson, D. D. 1988 The effects of knee brace hinge design and placement on joint mechanics. *J. Biomech.* **21**, 965–974. (doi:10.1016/0021-9290(88)90135-2)
28 Delp, S. L. 1990 Surgery simulation: a computer graphics system to analyze and design musculoskeletal reconstructions of the lower limb. PhD thesis, Stanford University, Stanford, CA.
29 Schutte, L. M. 1993 *Using musculoskeletal models to explore strategies for improving performance in electrical stimulation-induced leg cycle ergometry*. Stanford, CA: Stanford University.
30 Arnold, A. S., Salinas, S., Asakawa, D. J. & Delp, S. L. 2000 Accuracy of muscle moment arms estimated from MRI-based musculoskeletal models of the lower extremity. *Comput. Aided Surg.* **5**, 108–119. (doi:10.3109/10929080009148877)
31 Spoor, C. W. & van Leeuwen, J. L. 1992 Knee muscle moment arms from MRI and from tendon travel. *J. Biomech.* **25**, 201–206. (doi:10.1016/0021-9290(92)90276-7)
32 Grood, E. S., Suntay, W. J., Noyes, F. R. & Butler, D. L. 1984 Biomechanics of the knee-extension exercise. Effect of cutting the anterior cruciate ligament. *J. Bone Joint Surg. Am.* **66**, 725–734.
33 Anderson, D. E., Madigan, M. L. & Nussbaum, M. A. 2007 Maximum voluntary joint torque as a function of joint angle and angular velocity: model development and application to the lower limb. *J. Biomech.* **40**, 3105–3113. (doi:10.1016/j.jbiomech.2007.03.022)
34 Inman, V. T., Ralston, H. J. & Todd, F. 1981 *Human walking*. Baltimore, MD: Williams & Wilkins.
35 Cahalan, T. D., Johnson, M. E., Liu, S. & Chao, E. Y. 1989 Quantitative measurements of hip strength in different age groups. *Clin. Orthop. Relat. Res.* **246**, 136–145.
36 Murray, M. P., Gardner, G. M., Mollinger, L. A. & Sepic, S. B. 1980 Strength of isometric and isokinetic contractions: knee muscles of men aged 20 to 86. *Phys. Ther.* **60**, 412–419.
37 Marsh, E., Sale, D., McComas, A. J. & Quinlan, J. 1981 Influence of joint position on ankle dorsiflexion in humans. *J. Appl. Physiol.* **51**, 160–167.
38 van Eijden, T. M., Weijs, W. A., Kouwenhoven, E. & Verburg, J. 1987 Forces acting on the patella during maximal voluntary contraction of the quadriceps femoris muscle at different knee flexion/extension angles. *Acta. Anat. (Basel).* **129**, 310–314. (doi:10.1159/000146421)
39 Sale, D., Quinlan, J., Marsh, E., McComas, A. J. & Belanger, A. Y. 1982 Influence of joint position on ankle plantarflexion in humans. *J. Appl. Physiol.* **52**, 1636–1642.
40 Kadaba, M. P., Ramakrishnan, H. K. & Wootten, M. E. 1990 Measurement of lower extremity kinematics during level walking. *J. Orthop. Res.* **8**, 383–392. (doi:10.1002/jor.1100080310)
41 Lu, T. W. & O'Connor, J. J. 1999 Bone position estimation from skin marker co-ordinates using global optimisation with joint constraints. *J. Biomech.* **32**, 129–134. (doi:10.1016/S0021-9290(98)00158-4)
42 Delp, S. L., Anderson, F. C., Arnold, A. S., Loan, P., Habib, A., John, C. T., Guendelman, E. & Thelen, D. G. 2007 OpenSim: open-source software to create and analyze dynamic simulations of movement. *IEEE Trans. Biomed. Eng.* **54**, 1940–1950. (doi:10.1109/TBME.2007.901024)
43 Winter, D. A. 1991 *The biomechanics and motor control of human gait: normal, elderly, and pathological*, 2nd edn. Waterloo, Ontario: University of Waterloo Press.

44 Jonkers, I., Stewart, C. & Spaepen, A. 2003 The study of muscle action during single support and swing phase of gait: clinical relevance of forward simulation techniques. *Gait Posture* **17**, 97–105. (doi:10.1016/S0966-6362(02)00057-7)
45 Julian, F. J. & Morgan, D. L. 1979 Intersarcomere dynamics during fixed-end tetanic contractions of frog muscle fibres. *J. Physiol.* **293**, 365–378.
46 Burkholder, T. J. & Lieber, R. L. 2001 Sarcomere length operating range of vertebrate muscles during movement. *J. Exp. Biol.* **204**, 1529–1536.
47 Boakes, J. L. & Rab, G. T. 2006 Muscle activity during walking. In *Human walking* (eds J. Rose & J. G. Gamble), pp. 103–118. Baltimore, MD: Lippincott Williams and Wilkins.
48 Liu, M. Q., Anderson, F. C., Schwartz, M. H. & Delp, S. L. 2008 Muscle contributions to support and progression over a range of walking speeds. *J. Biomech.* **41**, 3243–3252. (doi:10.1016/j.jbiomech.2008.07.031)
49 Herzog, W. & Ter Keurs, H. E. 1988 Force–length relation of *in vivo* human rectus femoris muscles. *Pflugers Arch.* **411**, 642–647. (doi:10.1007/BF00580860)
50 Herzog, W., Guimaraes, A. C., Anton, M. G. & Carter-Erdman, K. A. 1991 Moment–length relations of rectus femoris muscles of speed skaters/cyclists and runners. *Med. Sci. Sports Exerc.* **23**, 1289–1296.
51 Rassier, D. E., MacIntosh, B. R. & Herzog, W. 1999 Length dependence of active force production in skeletal muscle. *J. Appl. Physiol.* **86**, 1445–1457.
52 Proske, U. & Morgan, D. L. 1987 Tendon stiffness: methods of measurement and significance for the control of movement. A review. *J. Biomech.* **20**, 75–82. (doi:10.1016/0021-9290(87)90269-7)
53 Lichtwark, G. A., Bougoulias, K. & Wilson, A. M. 2007 Muscle fascicle and series elastic element length changes along the length of the human gastrocnemius during walking and running. *J. Biomech.* **40**, 157–164. (doi:10.1016/j.jbiomech.2005.10.035)
54 Granzier, H. L., Akster, H. A. & Ter Keurs, H. E. 1991 Effect of thin filament length on the force–sarcomere length relation of skeletal muscle. *Am. J. Physiol.* **260**, C1060–C1070.
55 van den Bogert, A. J., Gerritsen, K. G. & Cole, G. K. 1998 Human muscle modelling from a user's perspective. *J. Electromyogr. Kinesiol.* **8**, 119–124. (doi:10.1016/S1050-6411(97)00028-X)
56 Blemker, S. S. & Delp, S. L. 2006 Rectus femoris and vastus intermedius fiber excursions predicted by three-dimensional muscle models. *J. Biomech.* **39**, 1383–1391. (doi:10.1016/j.jbiomech.2005.04.012)
57 Ettema, G. J. & Huijing, P. A. 1994 Effects of distribution of muscle fiber length on active length–force characteristics of rat gastrocnemius medialis. *Anat. Rec.* **239**, 414–420. (doi:10.1002/ar.1092390408)
58 Delp, S. L., Ringwelski, D. A. & Carroll, N. C. 1994 Transfer of the rectus femoris: effects of transfer site on moment arms about the knee and hip. *J. Biomech.* **27**, 1201–1211. (doi:10.1016/0021-9290(94)90274-7)